Universal scaling law in frictional non-Brownian suspensions

Frédéric Blanc, Enzo D'Ambrosio, Laurent Lobry, François Peters, and Elisabeth Lemaire*
Université Côte d'Azur, CNRS, InPhyNi-UMR 7010, 06108 Nice Cedex 2, France

(Received 5 January 2018; revised manuscript received 30 April 2018; published 30 November 2018)

We compare the rheology of two kinds of non-Brownian suspensions. One is made of spherical monodisperse polystyrene particles (80 μm in diameter), and the other is made of faceted sugar particles (average size, 100 μm), both suspended in a Newtonian silicon oil. We perform shear reversal experiments on both suspensions for several particle volume fractions, ϕ, and several shear stresses, τ. The two suspensions behave in a quite different fashion. For the faceted particle suspensions (FPSs), a large shear thinning is observed, while it is much more moderate for the spherical polystyrene particle suspensions (SPSs). Another striking difference lies in the value of the jamming packing fraction, ϕ_m, which is much lower for FPSs than for SPSs. Despite these differences, we will show that shear reversal experiments make it possible to obtain a universal scaling that holds for both FPSs and SPSs. In this scaling, the difference between the steady viscosity and the viscosity at the minimum that follows the shear reversal, normalized by the steady viscosity, is shown to depend only on the ratio $\phi/\phi_m(\tau)$. The collapse of all the data suggests that concentrated non-Brownian suspensions behave in a universal way regardless of the mechanisms responsible for flow hindering (rotation frustration or sliding friction).

DOI: 10.1103/PhysRevFluids.3.114303

I. INTRODUCTION

Non-Brownian suspensions are widespread in many industrial fields, e.g., paints, fresh concrete or food engineering, and natural flows, e.g., mud or lava flows or submarine avalanches, to mention but a few. In the past several years, active research has been carried out on the rheology of concentrated non-Brownian suspensions and has revealed the central role played by direct solid contact on the flow properties of suspensions. Boyer *et al.* [1] succeeded in applying a granular paradigm to describe the rheological behavior of non-Brownian and noncolloidal spheres suspended in a Newtonian fluid, showing the key role played by contact interactions between particles. The proliferation of frictional contacts is also known to be causing the discontinuous shear-thickening transition that is observed in very concentrated suspensions when the applied shear stress is high enough to overcome repulsive interactions between particles and to push them into contact [2–4]. These numerical and theoretical findings have been supported by macroscopic rheological measurements [5,6] as well as by atomic force microscopy measurements that directly relate the normal stress needed to enter the frictional regime at the nanoscale to the shear stress at which shear thickening occurs [7]. More generally, Guy *et al.* [8] proposed a constraint-based phenomenological model that, in addition to friction, enables accounting for more complex interactions between particles such as adhesion or rolling resistance. The authors show that all types of flow curves can be described by this model where constraints that are formed or released by stress are introduced.

*Corresponding author: elemaire@unice.fr

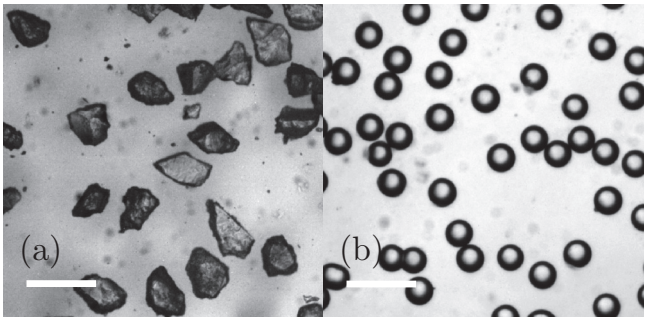

FIG. 1. (a) Sugar particles. (b) Polystyrene particles. Scale bar = 200 μm.

Coming back to basic frictional suspensions, the influence of solid friction between spherical particles on the rheology of non-Brownian suspensions has been extensively studied in the numerical work of Gallier *et al.* [9] where it is shown that microscopic friction between particles is a key parameter that governs the rheology of concentrated non-Brownian suspensions. To give an idea of the role played by solid friction between particles, the viscosity of a 45% suspension doubles when the friction coefficient, μ, is increased from 0 to 1. When the viscosity is split into hydrodynamic viscosity (ratio of the hydrodynamic stress to the shear rate) and contact viscosity (ratio of the contact stress to the shear rate), it is observed that the hydrodynamic viscosity hardly depends on the value of the friction coefficient while contact viscosity is highly sensitive to it [9]. As a consequence, when μ is varied from 0 to 0.5, at $\phi = 0.45$, the ratio of contact stress to hydrodynamic stress varies from 0.5 to 2. This great influence of the frictional properties of particles may be responsible for the scatter that is observed in experimental data that are found in literature when the variation of the viscosity with particle volume fraction is represented for suspensions made of different kinds of particles [10]. Some numerical studies [3,11,12] show that friction essentially changes the jamming fraction. Shear reversal experiments [13–15], numerical simulations [11,15,16], and theoretical modeling [17,18] have also been used to explore rheology of non-Brownian suspensions. As the shear is reversed, viscosity undergoes a steplike decrease, passes through a minimum, and increases again to reach the steady value it had before shear reversal. For suspensions of spherical particles, it has been shown that the difference between the steady viscosity, η_S, and the minimum viscosity, η_{min}, that follows the shear reversal is equal to 85% of the contact viscosity [11], which opens a way to estimate the value of contact viscosity upon performing shear reversal experiments.

In this article, we compare the rheology of two kinds of suspensions. One is made of spherical monodisperse polystyrene particles (SPSs) and the other is made of faceted sugar particles (FPSs), both suspended in a Newtonian silicon oil. In Sec. II we present the experimental systems and the experimental procedure. In Sec. III we present the main results and show that although these two suspensions exhibit quite different flow properties, their rheological behavior can be unified when the difference between the steady and the minimum viscosity normalized by the total shear viscosity is plotted against the ratio of the particle volume fraction to the jamming volume fraction.

II. EXPERIMENTS

A. Suspensions

The faceted particles are commercial crystal sugar particles [Fig. 1(a)]. Their density is measured to be 1.41 g/cm^3. The particles are sieved between 80 and 100 μm in order to reduce the initially large size distribution. Their mean aspect ratio, $< r > \approx 1.5$, has been evaluated by quantitative image analysis (see the Appendix). The spherical particles [Fig. 1(b)] are nominally monodisperse polystyrene particles (Microbeads TS 80), 80 μm in diameter and with a density of 1.05 g/cm^3.

The polystyrene particles are rinsed several times with distilled water, vacuum filtered, and finally carefully dried in an oven at 60 °C. Sugar and polystyrene particles are both dispersed in a Newtonian silicon oil (Rhodorsil 47 V1000) with density $\rho = 0.97\,\mathrm{g/cm^3}$ and viscosity of 0.98 Pa·s at $T = 23\,^{\circ}\mathrm{C}$. Particles are introduced in the silicon oil, and the suspension is carefully mixed. Then, air bubbles are removed by exposing the suspension to a vacuum. At last, the suspension is gently stirred in order to resuspend the particles that would have settled during the degassing procedure.

B. Rheometry experiments

Rheometric experiments were carried out in a controlled-stress rheometer Mars II (Thermofisher) with smooth rotating parallel plates (radius $R = 30\,\mathrm{mm}$, gap height $h = 2\,\mathrm{mm}$). Parallel rotating disk geometry is chosen because there is no or weak shear-induced particle migration in such a torsional flow [19,20]. The drawback is that shear rate is not constant in the gap but increases from 0 at the center to $\dot{\gamma}_R = \Omega R/h$ at the rim, Ω being the angular velocity of the rotating plate. To take into account this shear rate variation in the determination of the viscosity, η_{susp} that is a function of shear rate, we use the well-known Mooney-Rabinovitch correction:

$$\eta_{susp} = \eta_{app}\left[1 + \frac{1}{4}\frac{d\,\ln(\eta_{app})}{d\,\ln(\dot{\gamma}_R)}\right], \tag{1}$$

where η_{app} is the apparent viscosity measured by the rheometer:

$$\eta_{app} = \frac{2}{\pi R^3}\frac{\Gamma}{\dot{\gamma}_R}, \tag{2}$$

with Γ being the applied torque.

The plate surfaces are smooth and we have checked that there was no wall slip by changing the gap between the disks. The value of the measured viscosity is found not to depend on the gap height, which indicates that there is not any detectable wall slip [21]. Shear reversal tests were performed for various shear stress values, τ, between 10 and 100 Pa for FPSs and 5 and 100 Pa for SPSs (see the Supplemental Material for details on the protocol [22]). The particle packing fractions, ϕ, are in the range 0.3–0.47 for FPSs and 0.3–0.51 for SPSs. Within these conditions, the Reynolds number is small enough for inertial effects to be negligible, $\mathrm{Re} = \frac{\rho\tau h^2}{\eta^2} < 0.1$, and the Péclet number high enough to neglect Brownian effects, $\mathrm{Pe} = \frac{6\pi\tau a^3}{k_B T} > 10^9$.

III. RESULTS AND DISCUSSION

Figure 2 gives an example of the transient response of both suspensions for $\phi = 0.43$ where the reduced viscosity (suspension viscosity, η_{susp}, normalized by the suspending liquid viscosity, η_0) corrected with the Mooney-Rabinovitch method [Eq. (1)] is plotted against the accumulated strain from the shear reversal at the rim, γ. As already observed, shear reversal is accompanied by a steplike decrease of the viscosity. Then the viscosity continues to decrease, passes through a minimum, η_{min}, and increases again to reach the value it had before shear reversal, η_S. This is the behavior observed in all shear reversal experiments [13,14] and in simulations [11,16]. Ness *et al.* (2016) and Peters *et al.* (2016) showed that the transient response is the result of two contributions: the contact viscosity which vanishes almost instantaneously after the shear reversal and the hydrodynamic viscosity which almost instantaneously increases at shear reversal and then decreases much more slowly. Inspection of Fig. 2 shows that the steady (reduced) viscosity is much higher for FPSs than for SPSs, while the viscosity values of the two suspensions are not that different at the minimum. The observation that the steady viscosity is higher for FPSs than for SPSs has already been reported by several authors [23–25]—even though, in these papers, the particle aspect ratio is often much higher than 1—but shear reversal experiments give more information on the mechanisms through which particle shape affects suspension rheology. For SPSs, it has been shown

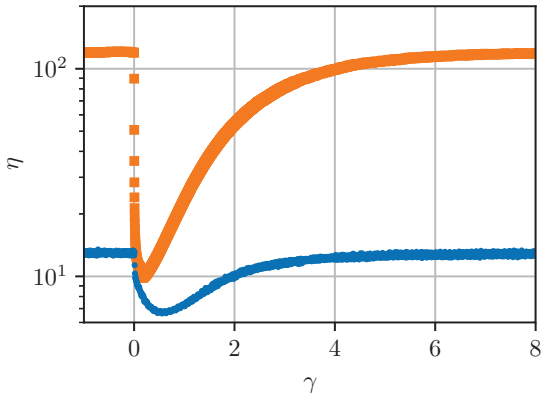

FIG. 2. Transient response of the viscosity under shear reversal. The reduced viscosity is plotted against the accumulated strain after shear reversal. Orange squares: Sugar particle suspension (FPS). Blue disks: polystyrene particle suspension (SPS). $\phi = 0.43$ and $\tau = 28\,\text{Pa}$.

that this kind of rheometric test provides a way to split the viscosity into hydrodynamic and contact contributions. This idea was first proposed by Lin *et al.* [15], and later Peters *et al.* [11] established a correlation according to which the difference between the steady viscosity and the viscosity at the minimum is equal to 85% of the contact viscosity. Then inspection of Fig. 2 [see also Figs. 3(c) and 3(d)] suggests that the hydrodynamic contribution to the viscosity is roughly the same for both

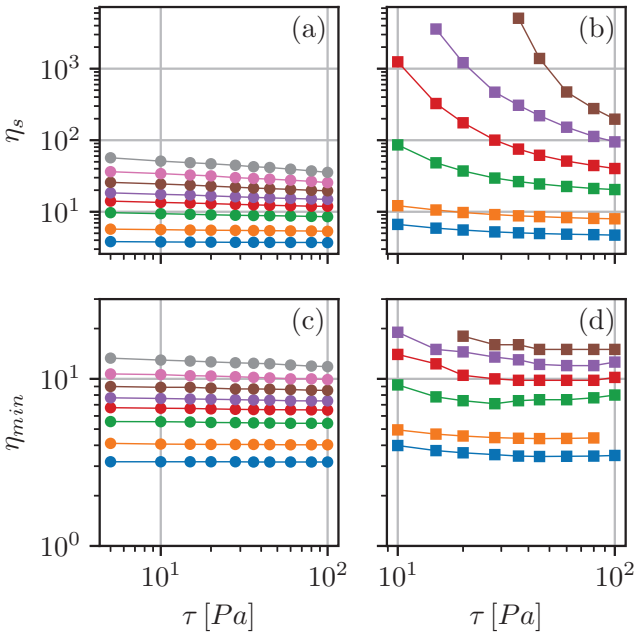

FIG. 3. The reduced viscosity curves as a function of shear stress for both FPSs (squares) and SPSs (disks). Blue: $\phi = 0.3$. Orange: $\phi = 0.35$. Green: $\phi = 0.40$. Red: $\phi = 0.43$. Purple: $\phi = 0.45$. Brown: $\phi = 0.47$. Pink: $\phi = 0.49$. Gray: $\phi = 0.51$. Steady viscosity of the SPSs (a) and FPSs (b). Viscosity at minimum of the SPSs (c) and FPSs (d). The sugar particle suspension exhibits a highly shear-thinning behavior, while the shear-thinning behavior demonstrated by the spherical particle suspension is much weaker. The viscosity at the minimum only slightly decreases with increasing shear stress for both FPSs and SPSs.

suspensions irrespective of the particle shape, faceted or spherical. Contrarily, the FPSs display a steady viscosity that is much higher than that of the SPSs, which suggests that the contact viscosity is greater for faceted particles than for spherical ones.

The experiment is repeated for several shear stresses and particle volume fractions. Figure 3 displays the variation of the steady viscosity, η_S, and of the viscosity at the minimum, η_{min}, with shear stress for the SPSs [Figs. 3(a) and 3(c), respectively] and for the FPSs [Figs. 3(b) and 3(d), respectively]. The minimum viscosity is almost constant with shear stress, while the steady viscosity decreases with increasing shear rate. Furthermore, the shear-thinning behavior of the steady viscosity is much more pronounced for the FPSs than for the SPSs. Shear thinning is common in frictional non-Brownian suspensions (see, for instance, Refs. [14,26–29]) though its physical origin is still debated. Weak adhesive forces between particles may cause shear thinning since they would lead to particle aggregation. In this scenario, suspensions are expected to exhibit a yield stress that may be understood as the minimum stress needed to break the aggregates and that makes the apparent viscosity decrease with the increase of shear stress. This explanation would be consistent with the observation that shear thinning is more pronounced in FPSs than in SPSs. In the former, the faceted shape of the particles favors Van der Waals interactions since it offers a much larger contacting surface between particles. The drawback of this explanation is that particle flocculation, if any, should also affect the viscosity at the minimum which thus would be stress-dependent. By contrast, the viscosity at the minimum is observed to hardly vary with shear stress. Furthermore, it can be seen by comparing Figs. 3(b) and 3(d) that, for the largest concentrations and the smallest stresses, it was possible to measure the viscosity at the minimum while the suspension is jammed ($\eta \longrightarrow \infty$) at steady state. However, even though, in this case, adhesive forces may not modify the mesoscopic structure of the suspensions, they may change the contact interactions between particles. It is thus possible that the adhesive forces exerted between the faceted particles participate in the marked shear thinning which is observed in FPSs since, as described in the introduction, the rheology of concentrated suspensions is very sensitive to contact forces. For SPSs, another mechanism has recently been proposed based on stress-induced variable friction between particles [30–32]. Chatté *et al.* [30] studied the second shear-thinning regime that occurs after the shear-thickening transition in a concentrated suspension of PVC particles dispersed in a plasticizer. In this frictional regime, the authors show using atomic force microscopy measurements that the friction coefficient decreases as the normal load increases, and they relate this decrease of the microscopic friction to the shear-thinning behavior. As for FPSs, however, the fine mechanisms leading to the marked shear-thinning behavior exhibited remain to be discovered and are expected to be more complicated than in the case of SPSs.

More generally, suspensions with rate-dependent viscosity are frequently encountered in either a Brownian [33–35] or non-Brownian regime [5,27,36]. It has been shown that rheology was well captured by introducing a stress-dependent jamming volume fraction. Without making any assumption about the underlying microscopic mechanisms, we follow this approach and define ϕ_m for each fixed shear stress value. For this purpose, the variation of the reduced viscosity with packing fraction is fitted to a modified Maron-Pierce law, *for each value of the shear stress*:

$$\eta_S = \frac{\alpha_0(\tau)}{\left[1 - \frac{\phi}{\phi_m(\tau)}\right]^2}, \tag{3}$$

where $\phi_m(\tau)$ is the jamming packing fraction at a given τ. We recall that, in the original Maron-Pierce equation, $\alpha_0 = 1$. Here α_0 is a second fitting parameter which is needed to obtain an accurate fit of the experimental data, especially for the FPSs. Its physical meaning, if any, is not clear, and α_0 should be seen only as a fitting parameter whose introduction makes sense only for concentrated suspensions since for $\phi \to 0$, η_S obviously tends toward 1. For very dilute suspensions, it has been shown experimentally and theoretically that the intrinsic viscosity, $[\eta] = \lim_{\phi \to 0} \frac{\eta_S - 1}{\phi}$, of a suspension of cubes differs from that of a suspension of spheres [37]. This is even less surprising that, for concentrated suspensions, the original Maron-Pierce relation cannot be applied rigidly. To deduce

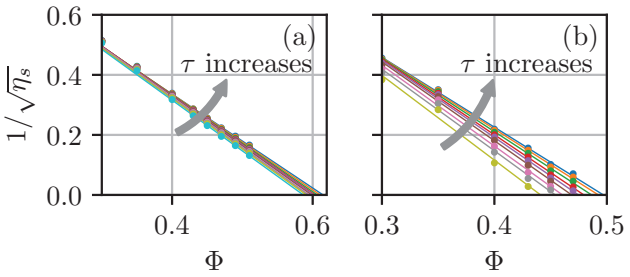

FIG. 4. The inverse of the square root of the reduced steady viscosity as a function of particle volume fraction for all the tested stresses. Each color corresponds to a given stress ($\tau \in [5\,\text{Pa} - 100\,\text{Pa}]$ for SPSs and $\tau \in [10\,\text{Pa} - 100\,\text{Pa}]$ for FPSs). (a) SPSs, (b) FPSs. Symbols: experimental data. Solid lines: fits.

the parameters α_0 and ϕ_m, we plot the inverse of the square root of the steady viscosity with packing fraction for all values of the tested shear stresses [see Fig. 4(a) for SPSs and Fig. 4(b) for FPSs]. The fit of each of these curves for $\phi \geqslant 0.4$ for SPSs and $\phi \geqslant 0.3$ for FPSs provides the values of ϕ_m and α_0 for each applied shear stress. As the shear stress decreases, the slope becomes larger in magnitude, and the jamming fraction decreases (see the Supplemental Materials for further details on fits and uncertainties [22]). Figure 5 displays the variation of these two parameters with τ. As expected, the jamming packing fraction is smaller for FPSs than for SPSs. This is consistent with what is observed in granular media where the maximum packing fraction decreases as the grain angularity increases (see, for instance, Refs. [38,39]). The values of ϕ_m measured for SPSs [0.59 – 0.615] are in the typical range that is reported in the literature for suspensions of frictional non-Brownian spheres [1,11,12,26,40]. For FPSs, ϕ_m lies in the range 0.43 to 0.50, which is of the same order as the jamming fraction fraction measured by Hafid *et al.* for suspensions of faceted river sand particles with an aspect ratio of 1.5 ($\phi_m \simeq 0.45$) [41].

The two kinds of suspensions appear to behave in a way that is quantitatively different: FPSs are much more shear thinning than SPSs and exhibit much lower maximum packing fractions, and the question arises whether it is possible to unify their behavior. It is sometimes proposed that the viscosity of non-Brownian suspensions depends only on the ratio of ϕ/ϕ_m (see, for instance, Ref. [42] or [43]). Rather, our results displayed in Fig. 6 show that this collapse is quite poor. For the

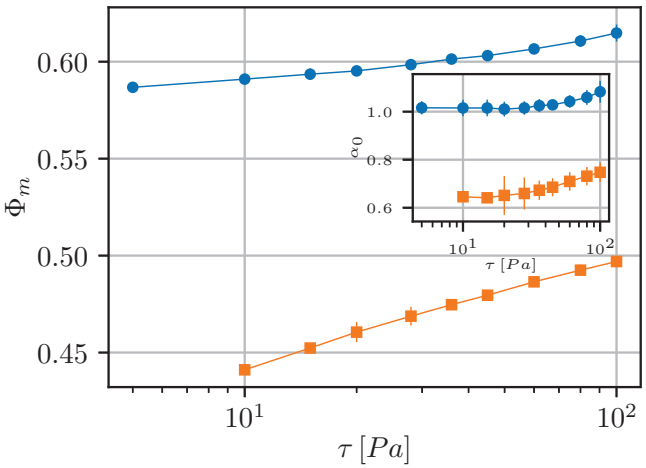

FIG. 5. Variation of the jamming packing fraction with the shear stress for FPSs (orange squares) and SPSs (blue disks). Insert: Variation of α_0 with τ.

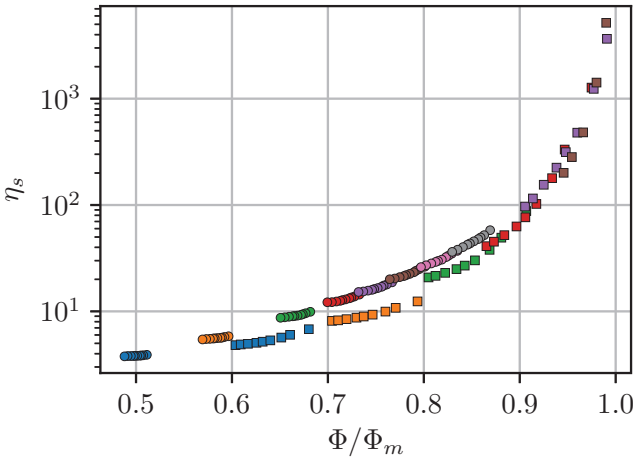

FIG. 6. Steady viscosity as a function of ϕ/ϕ_m. Squares: Sugar particles. Disks spherical polystyrene particles. Blue: $\phi = 0.3$. Orange: $\phi = 0.35$. Green: $\phi = 0.40$. Red: $\phi = 0.43$. Purple: $\phi = 0.45$. Brown: $\phi = 0.47$. Pink: $\phi = 0.49$. Gray: $\phi = 0.51$.

same ratio ϕ/ϕ_m, the steady viscosity of FPSs is lower than that of SPSs. Furthermore, even when the two suspensions are considered separately, the steady viscosity data, obtained for one kind of particles, are far from defining a unique curve when plotting against the ratio $\phi/\phi_m(\tau)$. Nevertheless, if rather than the steady viscosity, the ratio of the difference between the steady and the minimum viscosity to the steady viscosity, $(\eta_S - \eta_{min})/\eta_S$, is plotted against the ratio of the packing fraction to the maximum packing fraction, ϕ/ϕ_m, all measurements obtained for both the SPSs and the FPSs for all packing fractions and all shear stresses collapse onto a single curve. Figure 7 displays these

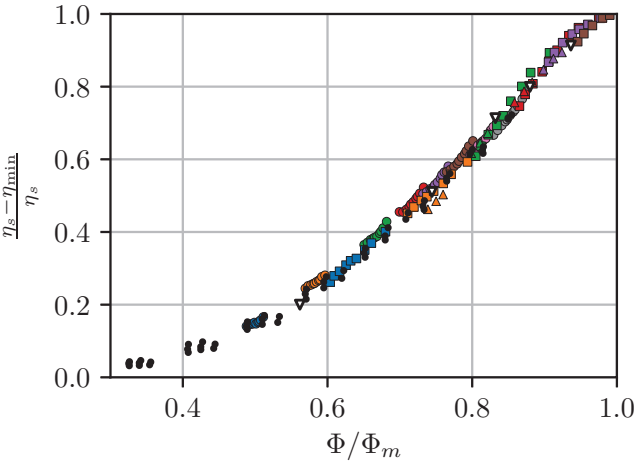

FIG. 7. Ratio of the difference between the steady viscosity and the viscosity at minimum normalized by the steady viscosity as a function of the ratio ϕ/ϕ_m. Squares: FPSs, disks: SPSs. Blue: $\phi = 0.3$. Orange: $\phi = 0.35$. Green: $\phi = 0.40$. Red: $\phi = 0.43$. Purple: $\phi = 0.45$. Brown : $\phi = 0.47$. Pink: $\phi = 0.49$. Gray: $\phi = 0.51$. Black disks: numerical simulations from Ref. [11] obtained for different sliding friction coefficients between 0 and 1 (no rolling friction). Empty triangles: PMMA particles 31 μm in diameter (Microbeads, CA30), dispersed in a Newtonian liquid from [13] ($\phi_m = 0.534$). Solid triangles: polyamideparticles (see Supplemental Materials [22])

results together with the numerical simulations of shear reversal of Peters *et al.* [11] performed for spherical particles with several sliding friction coefficients between 0 and 1 and with experimental data of Blanc *et al.* obtained with suspensions of PMMA spherical particles [13]. We have also tested this scaling with a highly polydisperse suspension made of irregular faceted polyamide particles (average diameter 15 μm) dispersed in a different silicon oil (see the Appendix for the description of the system). Again, the results collapse on the master curve (solid triangles in Fig. 7).

Recalling that, in the case of non-Brownian suspensions of spherical particles, the difference between the steady viscosity and the viscosity at the minimum is an estimate of the contact contribution to the viscosity [11], the collapse obtained for spherical particles suggests that a universal scaling can be obtained when the contact viscosity, η^C, normalized by the steady viscosity is plotted against the ratio $\phi/\phi_m(\tau)$. Concerning the suspensions of irregularly shaped particles, there is no proof that the difference between the steady and the minimum viscosity amounts to 85% of the contact viscosity. However, the comparison of Figs. 3(c) and 3(d) shows that the minimum viscosity of FPSs is not that different from that of SPSs, suggesting that, for FPSs, the minimum viscosity is roughly the hydrodynamic viscosity, η^H, as is the case for SPSs for which $\eta_{min} = \eta^H + 0.15\eta^C$ [11]. It should be noted that it is not surprising that the hydrodynamic viscosity does not much depend on the precise shape of the particles and should be almost the same for polyhedral or spherical particles provided that the aspect ratio is close to one. Identifying η_{min} and η^H would mean that the difference between η_S and η_{min} is also an estimate of the contact viscosity for FPSs. Following this conjecture, it appears that, for a given particle volume fraction, the contact viscosity is much higher for FPSs than for SPSs. This could probably be explained by the contact properties that should be different in the two suspensions. On the one hand, it has been shown that the contact viscosity of SPSs is very sensitive to the friction coefficient between particles. On the other hand, in the case of dry granular media, Estrada *et al.* [44] showed from 2D numerical simulations that the main effect of particle angularity is to hinder rotation and that this rotation frustration is somehow equivalent to some rolling resistance in an assembly of circular particles. Thus, the collapse of Fig. 7 suggests that regardless of the microscopic contact properties, the relative contribution of the contacts to the viscosity (η^C/η_S) is a function of the unique variable ϕ/ϕ_m.

IV. CONCLUSION

To conclude, we have shown that suspensions of spherical particles (SPSs) and of faceted particles (FPSs) with an aspect ratio close to one behave in a quite different fashion. At a given particle volume fraction, FPSs have a steady viscosity much higher than SPSs and are also much more shear thinning. These differences are rationalized in terms of a jamming packing fraction, $\phi_m(\tau)$, that is lower and more rapidly changing with shear stress for FPSs than for SPSs. Despite the tremendous differences observed in SPS and FPS behaviors, shear reversal experiments offer a unified framework for the rheology of suspensions based on either spherical or irregular-shaped particles. The ratio of the difference between the steady and the minimum viscosity (which is equal to 85% of the contact viscosity for SPSs and may be also an estimate of the contact viscosity for FPSs) to the steady viscosity depends only on the ratio ϕ/ϕ_m and defines a unique curve where the data obtained with both suspensions collapse. This scaling also collapses the results obtained with a highly polydisperse suspension of irregular polyamide particles, the numerical data of Peters *et al.* for rough frictional spherical particles [11] obtained for different friction coefficients ranging from 0 to 1, and the experimental data of Blanc *et al.* [13]. This scaling seems to be valid as long as the particle aspect ratio is close to one, regardless of size (in the non-Brownian limit), polydispersity, and shape of the particles. At a given ϕ, particle shape essentially affects the contact contribution to the viscosity, and the relative contact contribution to the viscosity can be simply described by a change in ϕ_m. Finally, introducing a shear stress-dependent jamming fraction, $\phi_m(\tau)$, enables us to capture the shear-thinning behavior of both suspensions. A possible interpretation of the increase of ϕ_m as the shear stress increases is a decrease of the friction coefficient between

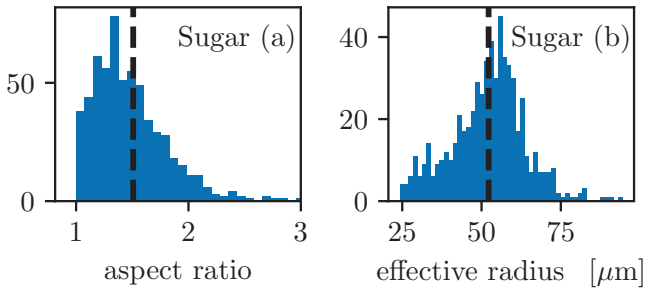

FIG. 8. (a) Aspect ratio distribution. (b) Equivalent size distribution.

particles as already measured by Chatté and explored in detail [32] for spherical particles. It is likely that the microscopic mechanisms involved in the variation of ϕ_m with stress are much more complicated in the case of FPSs. In particular, adhesion, which is favored by the flat surfaces of the particles, is likely to play a role in the flow hindrance since adhesive forces between faceted particles may increase significantly the rolling resistance that is already generated by the particle shape. It would be interesting to perform numerical simulations that include both sliding friction and rolling resistance between spherical particles in order to test if it is possible to capture the behavior of suspensions of angular-shaped particles as has been shown in 2D dry granular media by Estrada *et al.* [44].

Finally, from a practical point of view, the existence of the universal scaling depicted above opens the possibility of inferring the jamming packing fraction of a non-Brownian suspension from only one shear reversal experiment without varying particle concentration.

ACKNOWLEDGMENTS

We warmly thank Stany Gallier for fruitful discussions. This work was granted access to the HPC and visualization resources of the Centre de Calcul Interactif hosted by the Université Nice Sophia Antipolis.

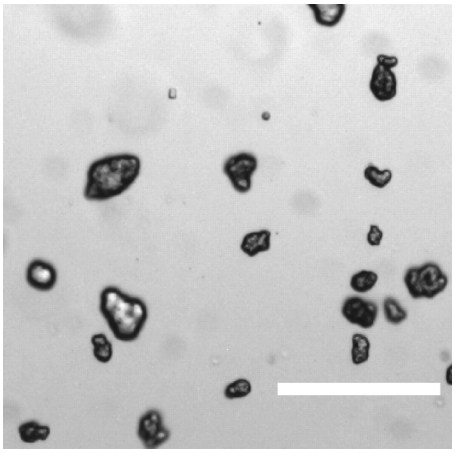

FIG. 9. Polyamide particles. Scale bar = 100 μm.

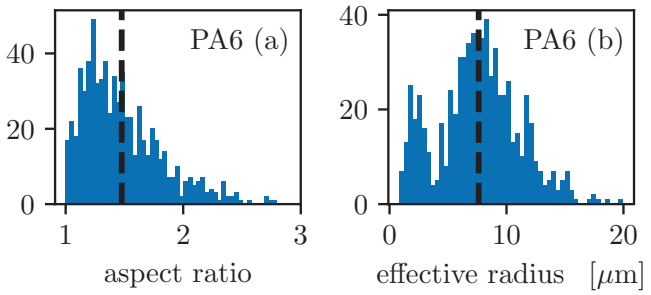

FIG. 10. (a) Aspect ratio distribution. (b) Equivalent size distribution.

APPENDIX: EXPERIMENTAL SYSTEMS AND PROCEDURE

1. Sugar particles

The size and aspect ratio distributions are determined by image processing. Figure 8 displays the aspect ratio distribution [Fig. 8(a)] and the equivalent radius distribution [Fig. 8(b)]. The equivalent radius is the radius of a disk that has the same area as the particles: $a_{eff} = \sqrt{\frac{\text{area}}{\pi}}$.

2. Suspensions of polyamide particles

We also tested the scaling presented in Fig. 6 with suspensions made of polyamide particles (Polyamide-Nylon 6 Powder PA 6, Goodfellow) dispersed in a silicon oil of viscosity 0.47 Pa·s at $T = 23\,^{\circ}$C. Four particle fractions were studied: $\phi = [0.37,\ 0.40,\ 0.43,\ 0.45]$. Figure 9 displays a picture of the polyamide particles that are very polydisperse with an average equivalent diameter ($\sim 15\ \mu$m) much smaller than that of the TS80 or sugar particles. Their shape is quite irregular, and they are neither as spherical as the polystyrene particles TS80 that have been used nor as sharp faceted as the sugar particles (see Fig. 1).

The histograms of aspect ratio and size distributions are displayed in Fig. 10.

[1] F. Boyer, É. Guazzelli, and O. Pouliquen, Unifying Suspension and Granular Rheology, Phys. Rev. Lett. **107**, 188301 (2011).

[2] R. Seto, R. Mari, J. F. Morris, and M. M. Denn, Discontinuous Shear Thickening of Frictional Hard-Sphere Suspensions, Phys. Rev. Lett. **111**, 218301 (2013).

[3] R. Mari, R. Seto, J. F. Morris, and M. M. Denn, Shear thickening, frictionless and frictional rheologies in non-Brownian suspensions, J. Rheol. **58**, 1693 (2014).

[4] M. Wyart and M. E. Cates, Discontinuous Shear Thickening without Inertia in Dense Non-Brownian Suspensions, Phys. Rev. Lett. **112**, 098302 (2014).

[5] B. M. Guy, M. Hermes, and W. C. K. Poon, Towards a Unified Description of the Rheology of Hard-Particle Suspensions, Phys. Rev. Lett. **115**, 088304 (2015).

[6] J. R. Royer, D. L. Blair, and S. D. Hudson, Rheological Signature of Frictional Interactions in Shear Thickening Suspensions, Phys. Rev. Lett. **116**, 188301 (2016).

[7] J. Comtet, G. Chatté, A. Niguès, L. Bocquet, A. Siria, and A. Colin, Pairwise frictional profile between particles determines discontinuous shear thickening transition in non-colloidal suspensions, Nat. Commun. **8**, 15633 (2017).

[8] B. M. Guy, J. A. Richards, D. J. M. Hodgson, E. Blanco, and W. C. K. Poon, Constraint-Based Approach to Granular Dispersion Rheology, Phys. Rev. Lett. **121**, 128001 (2018).

[9] S. Gallier, E. Lemaire, F. Peters, and L. Lobry, Rheology of sheared suspensions of rough frictional particles, J. Fluid Mech. **757**, 514 (2014).
[10] C. Chang and R. L. Powell, Effect of particle size distributions on the rheology of concentrated bimodal suspensions, J. Rheol. **38**, 85 (1994).
[11] F. Peters, G. Ghigliotti, S. Gallier, F. Blanc, E. Lemaire, and L. Lobry, Rheology of non-Brownian suspensions of rough frictional particles under shear reversal: A numerical study, J. Rheol. **60**, 715 (2016).
[12] A. Singh, R. Mari, M. M. Denn, and J. F. Morris, A constitutive model for simple shear of dense frictional suspensions, J. Rheol. **62**, 457 (2018).
[13] F. Blanc, F. Peters, and E. Lemaire, Local transient rheological behavior of concentrated suspensions, J. Rheol. **55**, 835 (2011).
[14] F. Gadala-Maria and A. Acrivos, Shear-induced structure in a concentrated suspension of solid spheres, J. Rheol. **24**, 799 (1980).
[15] N. Y. C. Lin, B. M. Guy, M. Hermes, C. Ness, J. Sun, W. C. K. Poon, and I. Cohen, Hydrodynamic and Contact Contributions to Continuous Shear Thickening in Colloidal Suspensions, Phys. Rev. Lett. **115**, 228304 (2015).
[16] C. Ness and J. Sun, Two-scale evolution during shear reversal in dense suspensions, Phys. Rev. E **93**, 012604 (2016).
[17] R. N. Chacko, R. Mari, S. M. Fielding, and M. E. Cates, Shear reversal in dense suspensions: The challenge to fabric evolution models from simulation data, J. Fluid Mech. **847**, 700 (2018).
[18] O. Ozenda, P. Saramito, and G. Chambon, A new rate-independent tensorial model for suspensions of noncolloidal rigid particles in Newtonian fluids, J. Rheol. **62**, 889 (2018).
[19] A. W. Chow, S. W. Sinton, J. H. Iwamiya, and T. S. Stephens, Shear-induced particle migration in Couette and parallel-plate viscometers: NMR imaging and stress measurements, Phys. Fluids **6**, 2561 (1994).
[20] D. Merhi, E. Lemaire, G. Bossis, and F. Moukalled, Particle migration in a concentrated suspension flowing between rotating parallel plates: Investigation of diffusion flux coefficients, J. Rheol. **49**, 1429 (2005).
[21] A. Yoshimura and R. K. Prud'homme, Wall slip corrections for Couette and parallel disk viscometers, J. Rheol. **32**, 53 (1988).
[22] See Supplemental Material at http://link.aps.org/supplemental/10.1103/PhysRevFluids.3.114303 for the experimental procedure is described in the first part and the raw data of the variation of the viscosity with shear stress and particle volume fraction are given in the second part.
[23] T. Kataoka, T. Kitano, Y. Oyanagi, and M. Sasahara, Viscous properties of calcium carbonate filled polymer melts, Rheol. Acta **18**, 635 (1979).
[24] L. Arbaret, M. Bystricky, and R. Champallier, Microstructures and rheology of hydrous synthetic magmatic suspensions deformed in torsion at high pressure, J. Geophys. Res.: Solid Earth **112**, 208 (2007).
[25] H. M. Mader, E. W. Llewellin, and S. P. Mueller, The rheology of two-phase magmas: A review and analysis, J. Volcanol. Geotherm. Res. **257**, 135 (2013).
[26] I. E. Zarraga, D. A. Hill, and D. T. Leighton Jr., The characterization of the total stress of concentrated suspensions of noncolloidal spheres in Newtonian fluids, J. Rheol. **44**, 185 (2000).
[27] A. Vázquez-Quesada, R. I. Tanner, and M. Ellero, Shear Thinning of Noncolloidal Suspensions, Phys. Rev. Lett. **117**, 108001 (2016).
[28] A. Vázquez-Quesada, A. Mahmud, S. Dai, M. Ellero, and R. I. Tanner, Investigating the causes of shear-thinning in non-colloidal suspensions: Experiments and simulations, J. Non-Newtonian Fluid Mech. **248**, 1 (2017).
[29] T. Dbouk, L. Lobry, and E. Lemaire, Normal stresses in concentrated non-Brownian suspensions, J. Fluid Mech. **715**, 239 (2013).
[30] G. Chatté, J. Comtet, A. Nigues, L. Bocquet, A. L. Siria, G. Ducouret, F. Lequeux, N. Lenoir, G. Ovarlez, and A. Colin, Shear thinning in non-Brownian suspensions, Soft Matter **14**, 879 (2017).
[31] R. I. Tanner, C. Ness, A. Mahmud, S. Dai, and J. Moon, A bootstrap mechanism for non-colloidal suspension viscosity, Rheol. Acta **57**, 635 (2018).

[32] L. Lobry, E. Lemaire, F. Blanc, S. Gallier, and F. Peters, Shear thinning in non-Brownian suspensions explained by variable friction between particles, J. Fluid Mech. (unpublished).
[33] C. R. Wildemuth and M. C. Williams, Viscosity of suspensions modeled with a shear-dependent maximum packing fraction, Rheol. Acta **33**, 421 (1984).
[34] J. C. Van der Werff and C. G. De Kruif, Hard-sphere colloidal dispersions: The scaling of rheological properties with particle size, volume fraction, and shear rate, J. Rheol. **33**, 421 (1989).
[35] D. Quemada, Rheological modeling of complex fluids. I. The concept of effective volume fraction revisited, Eur. Phys. J. Appl. Phys. **1**, (119) (1998).
[36] E. Brown, N. A. Forman, C. S. Orellana, H. Zhang, B. W. Maynor, D. E. Betts, J. M. DeSimone, and H. M. Jaeger, Generality of shear thickening in dense suspensions, Nat. Mater. **9**, 220 (2010).
[37] R. K. Mallavajula, D. L. Koch, and L. A. Archer, Intrinsic viscosity of a suspension of cubes, Phys. Rev. E **88**, 052302 (2013).
[38] E. Azéma, Y. Descantes, N. Roquet, J.-N. Roux, and F. Chevoir, Discrete simulation of dense flows of polyhedral grains down a rough inclined plane, Phys. Rev. E **86**, 031303 (2012).
[39] E. Azéma, N. Estrada, and F. Radjai, Nonlinear effects of particle shape angularity in sheared granular media, Phys. Rev. E **86**, 041301 (2012).
[40] G. Ovarlez, F. Bertrand, and S. Rodts, Local determination of the constitutive law of a dense suspension of noncolloidal particles through magnetic resonance imaging, J. Rheol. **50**, 259 (2006).
[41] H. Hafid, G. Ovarlez, F. Toussaint, P. H. Jezequel, and N. Roussel, Effect of particle morphological parameters on sand grains packing properties and rheology of model mortars, Cement Concrete Res. **80**, 44 (2016).
[42] M. Wang and J. F. Brady, Constant Stress and Pressure Rheology of Colloidal Suspensions, Phys. Rev. Lett. **115**, 158301 (2015).
[43] S. Mueller, E. W. Llewellin, and H. M. Mader, The rheology of suspensions of solid particles, Proc. R. Soc. London A **466**, 1201 (2009).
[44] N. Estrada, E. Azéma, F. Radjai, and A. Taboada, Identification of rolling resistance as a shape parameter in sheared granular media, Phys. Rev. E **84**, 011306 (2011).